

Truncation Correction for Non-horizontal Filter Lines

Stefan Hoppe, Joachim Hornegger, Günter Lauritsch, Frank Dennerlein, and Frédéric Noo

Abstract—State-of-the-art filtered backprojection (FBP) algorithms often define the filtering operation to be performed along non-horizontal filter lines in the detector. For non-horizontal filter lines, a limited scan field of view leads to axially as well as trans-axially truncated projections. In this work, we investigate the influence of axial and trans-axial data truncation on the reconstruction result and present two novel truncation correction methods which effectively handle both types of data truncation. Method 1 is a one-step approach which performs extrapolation along the filter lines to account for axial and trans-axial data truncation simultaneously. Method 2 consists of two steps: the first step handles trans-axial data truncation while axial data truncation is corrected during a modified forward rebinning step. Experiments are presented from simulated data of the FORBILD head phantom. The accurate M-line algorithm is used for reconstruction. Although the discussion is focused on accurate algorithms, the proposed truncation correction methods can be applied to any FBP algorithm.

Index Terms—Truncation Correction, Cone-beam Reconstruction, Computed Tomography.

I. INTRODUCTION

In computed tomography (CT), filtered backprojection algorithms involve a filtering step along predefined filter lines in the detector. Due to the global nature of the filter operation (Hilbert filter, Ramp filter), these filter lines must not be truncated to avoid severe reconstruction artifacts. Especially in C-arm CT, filter line truncation occurs quite frequently since the device has a limited detector size and therefore a limited scan field of view. We distinguish between axial and trans-axial data truncation. Trans-axial data truncation results from wide objects which are truncated in horizontal direction whereas axial data truncation results from long objects which are truncated in vertical direction. In a Feldkamp-type algorithm [1] for example, where filtering is performed along the detector rows, only trans-axial filter line truncation is possible. With the invention of new accurate and approximate cone-beam reconstruction algorithms together with the utilization of more exotic source trajectories, non-horizontal filter lines were introduced (see e.g. [2],[3],[4],[5]). Hence, axial data truncation becomes an issue. Even for methods which solve the long object problem, non-horizontal filter lines impose an unwanted restriction on the extend of the volume which can be reconstructed without artifacts.

S. Hoppe and J. Hornegger are with the Institute of Pattern Recognition (LME), University of Erlangen-Nuremberg, Erlangen, Germany.

F. Noo and F. Dennerlein are with the Department of Radiology (UCAIR), University of Utah, Salt Lake City, UT, USA.

G. Lauritsch is with the Siemens AG, Medical Solutions, Forchheim, Germany.

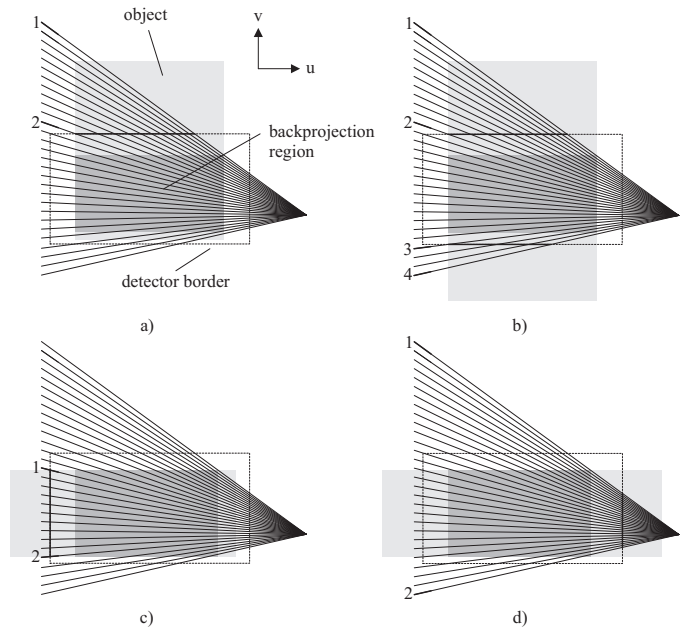


Fig. 1. Filter line truncation for the M-line algorithm where all filter lines intersect in a single point. a,b) Axially and c,d) trans-axially truncated projections. a) The filter lines between 1-2, b) between 1-2 and 3-4, c) between 1-2 and d) between 1-2 are truncated. Arbitrary combinations are possible.

In this work, we investigate the influence of axially and trans-axially truncated projections on the reconstruction result when dealing with non-horizontal filter lines. We present two novel methods to handle truncation problems for that case. Method 1 is a one-step approach which performs extrapolation along the filter lines to account for axial and trans-axial data truncation simultaneously. Method 2 consists of two steps: the first step handles trans-axial data truncation while axial data truncation is corrected during a modified forward rebinning step. The discussion is focused on the accurate M-line algorithm, originally presented in [6], but the results can easily be generalized to any FBP algorithm.

The paper is organized as follows. In Section II, we review the reconstruction process with a special focus on the filter operation to define the type of data truncation problem. Section III introduces our new methods. Experiments are presented in Section IV. Section V summarizes our results.

II. BACKGROUND AND PROBLEM DEFINITION

From an implementational point of view, accurate image reconstruction for a point \underline{x} inside the support of the object basically involves the following steps:

- (1) Differentiate the cone-beam data with respect to the source trajectory.
- (2) Perform forward rebinning from detector coordinates to filter line coordinates.
- (3) Perform one-dimensional Hilbert filtering along the filter lines.
- (4) Perform backward rebinning from filter line coordinates to detector coordinates.
- (5) Backproject the result into the image space.

If $g(s)$ identifies the (differentiated) cone-beam data for a given filter line, step (3) can be expressed as follows

$$g_F(s) = \int_{-\infty}^{+\infty} h_{hilb}(s - s')g(s')ds', \quad (1)$$

where $g_F(s)$ denotes the filtered data along the line, with the Hilbert kernel

$$h_{hilb}(s) = \frac{1}{\pi s}. \quad (2)$$

Since $h_{hilb}(s)$ has infinite support, the filter operation involves all values of $g(s)$ along the line. Data truncation now effectively amounts to multiplying $g(s)$ with a rectangular window in the spatial domain. This corresponds to a smearing of the spectrum of $g(s)$ and manifests in so called truncation artifacts in the final reconstructed image (Section IV demonstrates the effect). We define the problem of filter line truncation as follows: *any filter line that leaves the detector before it leaves the shadow of the object is a truncated filter line and leads to reconstruction artifacts for each point which projects onto it.* This implies, that although the point may be well inside the scan field of view and though Tuy's sufficiency theorem [7] may be fulfilled, it cannot be reconstructed exactly as long as it lies on any such truncated filter line.

Two cases can be distinguished: trans-axial data truncation results from wide objects which are truncated in horizontal direction whereas axial data truncation results from long objects which are truncated in vertical direction. With non-horizontal filter lines, both types may occur separately or simultaneously. Figure 1 displays several scenarios for filter lines proprietary to the M-line algorithm, where filtering is performed along the projection of so called M-lines (see [6] for details). By choosing the setup similar to [8], all filter lines converge to a common point, as depicted. Note that only points within the backprojection region need to be filtered.

III. TRUNCATION CORRECTION

Both proposed truncation correction methods build upon the so called water cylinder correction originally presented in [9]. It will therefore be reviewed shortly before presenting the new material. Note that in both methods, truncation correction is done solely for the purpose of filtering. No extrapolated value will ever be backprojected. Our methods can be applied, besides the M-line approach, to any FBP algorithm (there should of course be some oblique filter lines) e.g. the Katsevich circle-plus-line or circle-plus-arc algorithms [3],[4] or the ACE algorithm [5] which requires filtering on very oblique lines.

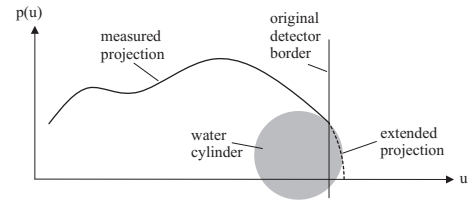


Fig. 2. Projection values $p(u)$ along one detector row with truncation at the right detector border. For each detector row and for each side of that row, the extend (midpoint and radius) of a 2D water cylinder is determined (see [9] for details).

A. Review: Water Cylinder Correction

This method is commonly used for the FDK algorithm to handle trans-axial data truncation. For each detector row and for each side of that row, the extend (midpoint and radius) of a 2D water cylinder is determined (Figure 2). The basic assumption of this method is that the missing portion of the object is well enough approximated by integrals along parallel lines through that water cylinder, disregarding the cone-beam nature of the beam. The method effectively removes the data discontinuities at the detector border and produces decreasing projection values for the missing part of the object.

B. Method 1: Extrapolation along Filter Lines

This method is a straight forward extension to the water cylinder correction for non-horizontal filter lines. While the water cylinder correction was initially developed for horizontal filter lines, the extension to oblique lines is made by applying it to each filter line, rather than to each detector row. Thus, axial as well as trans-axial data truncation can be corrected simultaneously within one processing step. The extended reconstruction algorithm comprises the following steps:

- (1) Perform forward rebinning.
- (2) Apply method 1.
- (3) Differentiate the cone-beam data.
- (4) Perform one-dimensional Hilbert filtering.
- (5) Perform backward rebinning.
- (6) Backproject the result into the image space.

Note the reversed order of the forward rebinning step since method 1 has to be applied before the differentiation step.

C. Method 2: Separate Axial and Trans-axial Extrapolation

This method consists of two steps. Step 1 handles trans-axial data truncation using the original water cylinder correction e.g. along the detector rows. Step 2 accounts for axial data truncation by filtering along lines with a kink, if these lines exceed the detector axially (Figure 3). When a line intersects the detector border, the samples are taken from the first or last detector row, respectively. This can be efficiently incorporated into a modified forward rebinning step. The method has the nice property that the projection values along the lines with the kink will always smoothly decrease towards zero because the water cylinder correction ensures that the projection values along the first and last row smoothly decrease towards zero. The extended reconstruction algorithm comprises the following steps:

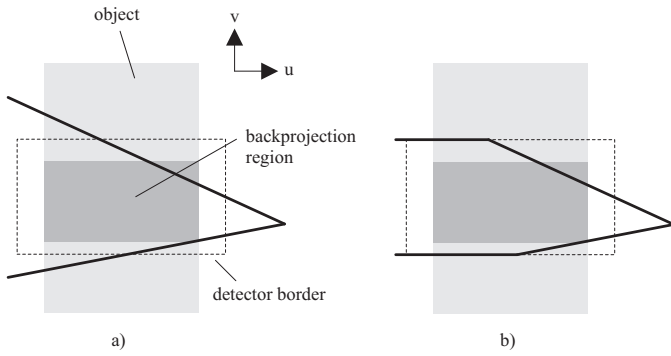


Fig. 3. Method 2: filtering is done along lines with a kink if these lines exceed the detector axially. a) Original filter lines. b) Corresponding filter lines with kink. The setup matches that of Figure 1b).

- (1) Apply method 2, step 1.
- (2) Differentiate the cone-beam data.
- (3) Apply method 2, step 2 (modified forward rebinning).
- (4) Perform one-dimensional Hilbert filtering.
- (5) Perform backward rebinning.
- (6) Backproject the result into the image space.

IV. EXPERIMENTS AND RESULTS

Experiments were done on simulated data of the FORBILD head phantom [10]. The data was collected along a short-scan-plus-arc trajectory. The radius was set to 750 mm, the source-to-detector distance was set to 1200 mm. The detector was simulated with 256^2 pixels (using 4×4 sub detector elements) with an isotropic resolution of 1.6 mm/pixel. The sampling rate was 0.4° /projection resulting in 500 projections for the short-scan and 58 projections for the arc-scan. The reconstructed volume has an isotropic resolution of 2.0 mm/voxel and is of dimension 128^3 voxels. We used the M-line algorithm [6] as a representative of the class of accurate algorithms. The point on the source trajectory, at which all M-lines intersect was positioned at 140° on the short-scan, measured from the start of the arc segment. This gives very oblique filter lines for the arc segment and for the first half of the short-scan but almost horizontal filter lines on the second half of the short-scan. Figure 4 shows the non-truncated reference images for comparison. Figure 5 shows how the projections were artificially truncated for the various experiments. The degree of truncation (DoT) is further quantified according to

$$DoT(\lambda) = (1 - N(\lambda)/N_0(\lambda)) \cdot 100, \quad (3)$$

where $N(\lambda)$ and $N_0(\lambda)$ count the number of non-zero detector pixels in the truncated and non-truncated case, respectively, and λ identifies the projection under consideration (Figure 6).

A. Trans-Axial Data Truncation

To simulate trans-axial data truncation, 25 detector columns at the left and right border of the projection images were set to zero as shown in Figure 5b). Figure 6a) shows the corresponding DoT. The results can be seen in Figure 7 (row 1). In a), the density values of the whole slice are disturbed

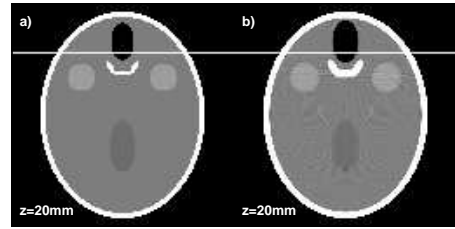


Fig. 4. Reference images. a) Ground truth. b) Reconstruction without truncation. The window was set to [1.01,1.09]. The white line indicates the location for the density profiles used throughout the experiments.

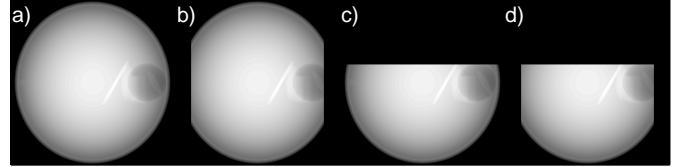


Fig. 5. Artificial truncation, shown exemplarily for the first projection along the short-scan. a) Original projection. b) Trans-axial data truncation. c) Axial data truncation. d) Combined data truncation.

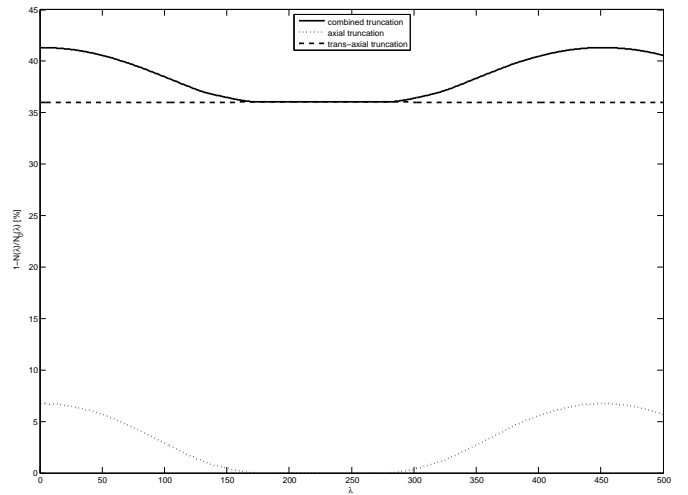


Fig. 6. DoT for a) trans-axial (dotted line), b) axial (dashed line) and c) combined data truncation (solid line). The mean DoT values are a) 3.07%, b) 36.00% and c) 38.51%.

severely. Moreover, the slice shows an extreme intensity drop-off. In b) and c), method 1 and method 2 restore the image quite well, except for some minor shadows next to the outer bone structure. Figure 8a) shows the corresponding density profiles along a selected line (cf. Figure 4).

B. Axial Data Truncation

To simulate axial data truncation, 100 detector rows at the top border of the projection images were set to zero as shown in Figure 5c). Figure 6b) shows the corresponding DoT. The results are displayed in Figure 7 (row 2). The dark shadow in d) clearly is a data truncation effect, arising from the introduced discontinuity of the projection data. Its location is a result of the chosen M-line configuration. In e) and f), this shadow is removed by method 1 and method 2 which perform almost identically. Figure 8b) shows the corresponding density

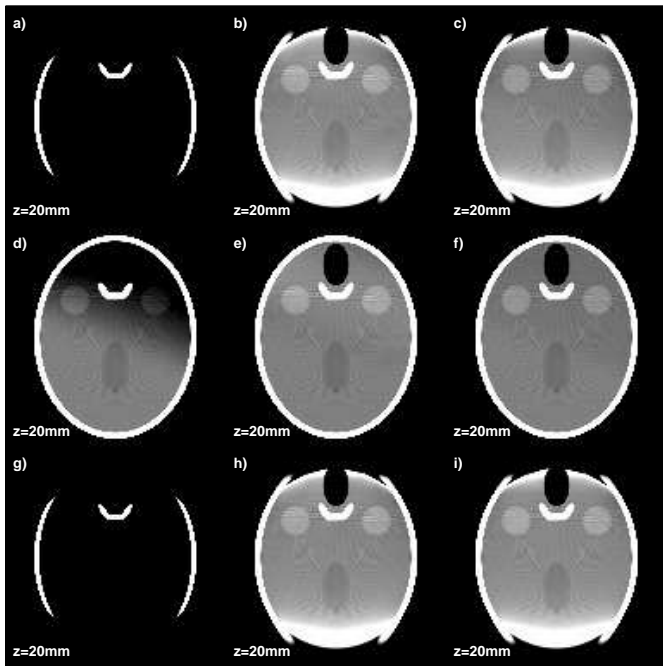


Fig. 7. Reconstruction results for trans-axial (row 1), axial (row 2) and combined (row 3) data truncation when using no truncation correction (column 1), using method 1 (column 2), using method 2 (column 3). The window was set to [1.01,1.09].

profiles along a selected line (cf. Figure 4).

C. Combined Data Truncation

To simulate combined data truncation, the images were truncated axially and trans-axially according to Figure 5d). Figure 6c) shows the corresponding DoT. Figure 7 (row 3) depicts the results. With no truncation correction in g), the outcome appears almost identical to the trans-axial truncation case a), since these artifacts are dominant. However, in fact, the artifacts are composed of both truncation types. In h) and i), method 1 as well as method 2 remove the shadows as expected. This confirms that the proposed methods can handle both types of data truncation, concurrently.

V. CONCLUSIONS

We have presented two methods to handle data truncation for non-horizontal filter lines. They can be applied to any FBP algorithm. The methods were tested on simulated data of the FORBILD head phantom. The results show that truncation effects resulting from very oblique lines can be removed effectively. Almost no difference with respect to image quality can be observed between method 1 and method 2. However, method 1 is computationally less efficient since it forces the differentiation to be performed on the rebinned cone-beam data rather than on the original cone-beam data as with method 2. This requires more operations since the number of filter lines is in general much higher than the number of detector rows. For this reason, we suggest to use method 2.

ACKNOWLEDGMENTS

This work was supported by Siemens AG, Medical Solutions.

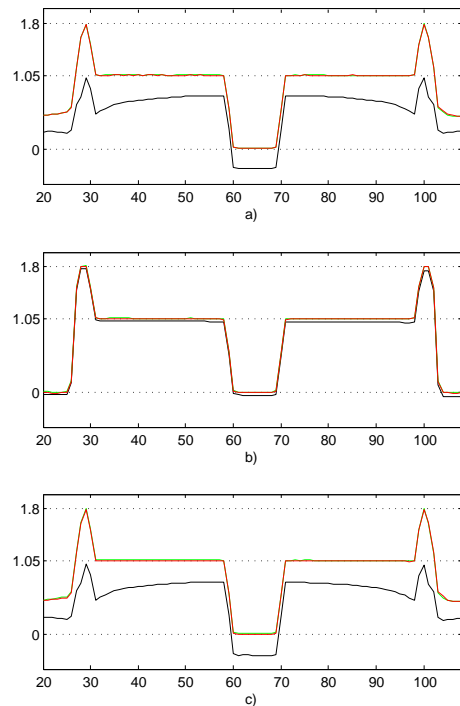


Fig. 8. Density profiles for trans-axial (row 1), axial (row 2) and combined (row 3) data truncation when using no truncation correction (black line), using method 1 (green line), using method 2 (red line).

REFERENCES

- [1] L.A. Feldkamp, L.C. Davis, and J.W. Kress. Practical cone-beam algorithm. *J. Opt. Soc. Am. A*, 1(6):612–619, 1984.
- [2] J. Pack, F. Noo, and H. Kudo. Investigation of saddle trajectories for cardiac ct imaging in cone-beam geometry. *Physics in Medicine and Biology*, 49(11):2317–2336, 2004.
- [3] A. Katsevich. Image reconstruction for the circle-and-line trajectory. *Physics in Medicine and Biology*, 49(22):5059–5072, 2004.
- [4] A. Katsevich. Image reconstruction for the circle-and-arc trajectory. *Physics in Medicine and Biology*, 50(10):2249–2265, 2005.
- [5] B.E. Nett, T. Zhuang, and G.-H. Chen. A cone-beam fbp reconstruction algorithm for short-scan and super-short-scan source trajectories. In *Fully 3D Image Reconstruction in Radiology and Nuclear Medicine*, pages 396–400, Salt Lake City, UT, USA, Jul. 6 - Jul. 9, 2005.
- [6] J. Pack and F. Noo. Cone-beam reconstruction using 1d filtering along the projection of m-lines. *Inverse Problems*, 21(3):1105–1120, 2005.
- [7] H.K. Tuy. An inversion formula for cone-beam reconstruction. *SIAM J. Appl. Math.*, 43(3):546–552, 1983.
- [8] S. Hoppe, F. Dennerlein, G. Lauritsch, J. Hornegger, and F. Noo. Cone-beam tomography from short-scan circle-plus-arc data measured on a c-arm system. *Nuclear Science Symposium Conference Record, 2006 IEEE*, 6:2873–2877, 2006.
- [9] J. Hsieh, E. Chao, J. Thibault, B. Grekowitz, A. Horst, S. McOlash, and T.J. Myers. A novel reconstruction algorithm to extend the ct scan field-of-view. *Medical Physics*, 31(9):2385–2391, 2004.
- [10] Description of the FORBILD Head Phantom, online at <http://www.imp.uni-erlangen.de/forbild/deutsch/results/head/head.html> (last visit Jan 07).